energies

MDPI

Article

Analysis of Radial Inflow Turbine Losses Operating with Supercritical Carbon Dioxide

Antti Uusitalo * and Aki Grönman

School of Energy Systems, LUT University, 53850 Lappeenranta, Finland; aki.gronman@lut.fi
* Correspondence: antti.uusitalo@lut.fi

Abstract: The losses of supercritical CO_2 radial turbines with design power scales of about 1 MW were investigated by using computational fluid dynamic simulations. The simulation results were compared with loss predictions from enthalpy loss correlations. The aim of the study was to investigate how the expansion losses are divided between the stator and rotor as well as to compare the loss predictions obtained with the different methods for turbine designs with varying specific speeds. It was observed that a reasonably good agreement between the 1D loss correlations and computational fluid dynamics results can be obtained by using a suitable set of loss correlations. The use of different passage loss models led to high deviations in the predicted rotor losses, especially with turbine designs having the highest or lowest specific speeds. The best agreement in respect to CFD results with the average deviation of less than 10% was found when using the CETI passage loss model. In addition, the other investigated passage loss models provided relatively good agreement for some of the analyzed turbine designs, but the deviations were higher when considering the full specific speed range that was investigated. The stator loss analysis revealed that despite some differences in the predicted losses between the methods, a similar trend in the development of the losses was observed as the turbine specific speed was changed.

Keywords: supercritical carbon dioxide; radial inflow turbine; turbine loss models; turbomachinery loss

check for updates

Citation: Uusitalo, A.; Grönman, A. Analysis of Radial Inflow Turbine Losses Operating with Supercritical Carbon Dioxide. *Energies* **2021**, *14*, 3561. https://doi.org/10.3390/en14123561

Academic Editors: Satoru Okamoto and Andrea De Pascale

Received: 5 May 2021
Accepted: 11 June 2021
Published: 15 June 2021

Publisher's Note: MDPI stays neutral with regard to jurisdictional claims in published maps and institutional affiliations.

Copyright: © 2021 by the authors. Licensee MDPI, Basel, Switzerland. This article is an open access article distributed under the terms and conditions of the Creative Commons Attribution (CC BY) license (https://creativecommons.org/licenses/by/4.0/).

1. Introduction

The use of supercritical carbon dioxide as the working fluid has been identified as a promising power generation technology candidate for producing electricity with reduced environmental impacts and high conversion efficiency. The supercritical CO_2 (SCO_2) power cycles have been identified as potential candidates for several applications such as future nuclear reactors, waste heat recovery, concentrating solar power as well as suggested as potential replacement technology for the steam turbine power cycles, including the typical large-scale fossil fuel power plants [1]. If the SCO_2 gas turbine technology is used together with oxy-combustion, large-scale power plants with extremely high efficiencies with full carbon capture could be realized [2].

It has been observed that the efficiency of the SCO_2 power cycle is highly affected by the efficiencies of turbines and the compressors of the cycle [3]. The cycle heat exchanger design has been also observed to have influence on the turbomachinery performance of SCO_2 power cycles as the pressure ratio over the turbomachines is influenced by the pressure drop over the heat exchangers [4]. To be able to maximize the power output and efficiency of SCO_2 power cycles it is highly important to investigate and increase the knowledge on the operation of the turbomachines operating with supercritical CO_2. In general, in large-scale systems, the axial [5] type of turbines have been often considered, whereas in smaller scale systems the radial inflow turbines, e.g., [6–8] have been considered as the most suitable turbine type for SCO_2 power cycles. In the indicative technological categorization for the SCO_2 turbogenerator technical solutions presented by Fuller et al. [9],

axial turbines and single shaft solutions have been recommended for about and above 10 MW scale SCO_2 systems, whereas the radial inflow turbines and multiple shaft process layouts have been considered as a more feasible choice for smaller scale SCO_2 power plants with power levels below 10 MW. In addition to the use of axial and radial types of turbines in SCO_2 applications, the use of radial outflow turbines has been investigated and proposed [10]. Lee et al. [11] evaluated suitable loss correlations for both axial and radial type of turbomachines including turbines and compressors. They highlighted that the accuracy of the existing correlations for predicting losses of different types SCO_2 turbomachines and designs should be further investigated and validated. In a recent review on SCO_2 technology, it is shown that most of the existing turbomachinery designs are for low power outputs of below 300 kW, whereas there are only a few systems in where MW scale turbomachines have been designed and constructed for SCO_2 power systems [12].

In this study, the analysis is concentrated on the radial-inflow type of turbines. In the literature, there are several studies investigating the design and performance of SCO_2 driven radial inflow turbines. Lv et al. [6] made an analysis on the design and loss distributions in SCO_2 radial inflow turbines. A comparison of 1D loss correlations with the computational fluid dynamics (CFD) analysis results with a turbine design having the specific speed close to 0.4 was carried out. Based on their results, a set of loss correlations was recommended that provided the highest accuracy in respect to the CFD results. Recently, Zhou et al. [7] investigated the performance and losses of a 1 MW SCO_2 radial turbine by using CFD analysis. The investigated turbine had the design specific speed of close to 0.3, based on the given turbine design values. Both the design and off-design conditions were investigated, and it was concluded that the turbine can reach high isentropic efficiencies at both design and off-design operating conditions. Turbine efficiency of above 85% was reported at the design conditions. They also observed that the tip clearance height had a notable effect on the efficiency. In a study by Qi et al. [8], SCO_2 radial turbine designs with power outputs of 100 kW and 200 kW were investigated. Turbine size parameters were used and efficiencies between 78% to 82% were reported. They also observed that the rotor passage loss is the source of the most significant losses in the investigated turbine expansion. In addition, the tip clearance loss and kinetic loss at the turbine exhaust were identified as significant sources of loss. In [13] isentropic efficiencies of 86% and 87% were reported for 178 kW and 213 kW power output SCO_2 turbines designed for an experimental facility. Holaind et al. [14] studied the design of small-scale SCO_2 centrifugal compressor and radial turbine by using the similarity approach and by using RANS CFD simulations for optimizing the 3D geometries. The analysis included the volute, stator and rotor. They observed an efficiency of about 70% at the nominal point for the investigated turbine and an efficiency of 76% for the compressor. Recently, Son et al. [15] investigated and developed and improved an off-design model for SCO_2 turbomachines by using the set of loss correlations and a 1D method proposed by KAIST. In the model, they combined the 1D method with pre-trained deep neural network for predicting the off-design performance of SCO_2 turbomachines.

The effect of specific speed (Ns) and power on geometry and loss distribution of supercritical CO_2-driven radial inflow turbines was recently studied in [16]. The analysis was based on the use of existing turbine loss correlations. The radial inflow turbine design with flow rates of 1 kg/s, 3 kg/s, 9 kg/s, and 25 kg/s were investigated with turbine operating conditions typically suggested for the recompression CO_2 cycles. The highest turbine efficiencies were predicted in the specific speed range of 0.5 to 0.6 which was in good agreement between the well-known Balje [17] and Rohlik [18] efficiency vs. specific speed graphs for generalized radial turbine designs. The highest turbine efficiencies were observed with slightly lower values of specific speed ranging from 0.2 to 0.5 in the recent study by Unglaube and Chiang [19] for 100 kW scale turbines. Lee and Gurgenci [20] investigated 300 kW, 1 MW, 10 MW and 20 MW turbines with equal design specific speeds. They used the Aungier's, Moustapha's, and Whitfield and Baines' methods for evaluating

turbine design and losses. Their study indicated that the Aungier's and Moustapha's models predicted comparable losses whereas slightly higher losses were predicted when following the design method by Whitfield and Baines. Persky et al. [21] investigated the design of a 30 MW scale radial turbine. They estimated a turbine efficiency of close to 90% for the turbine that was designed for a high temperature solar SCO_2 Brayton cycle. Keep [22] investigated low specific speed radial inflow turbines for SCO_2 power systems by using mean line design and CFD. In that study, it was observed that the efficiency of low specific speed turbine designs was highly influenced by the rotor-stator interspace.

The previous studies have shown that SCO_2 radial turbines are capable of reaching high efficiencies, ranging from about 80% to over 90%. In addition, the turbines are characterized by small dimensions together with the requirement of high rotational speeds, even at high power scales. Despite the previous studies on SCO_2 turbines, it is still unclear how accurate the different loss models are when predicting losses in SCO_2 radial turbines. Especially, the investigations on the accuracy of the models with different design specific speeds have not been fully studied in the present literature, as in most of the previous studies only a single turbine design speed or a very narrow design speed range has been considered and investigated (e.g., [6,7,20,22]). In addition, the final turbine design rotational speed is not often selected based only on the optimal turbine design, but also includes considerations on the mechanical design and it can be also influenced by the compressor design if the compressor and turbine are assembled on a single shaft. Thus, it is important to further investigate the applicability of the different existing loss models for predicting losses in radial turbines having different design rotation speeds (specific speeds). In the previous study by the authors [16], the 1D design of SCO_2 radial inflow turbines with different specific speeds was investigated and the method for defining the turbine geometry and losses was presented. However, in that study, the turbine loss estimation was based only on using the 1D design method and by considering only a single passage loss model and thus, the loss predictions were not compared against any other loss prediction methods. In this study, the expansion losses occurring in a 1 MW scale radial inflow-turbines operating with supercritical carbon dioxide are investigated by using different passage loss correlations and comparing the results of loss correlations to the results obtained by using computational fluid dynamics (CFD) simulations. The specific focus of the study is on identifying the effect of design specific speed on efficiency and loss distribution of SCO_2 radial inflow turbines with a turbine design mass flow rate of 9 kg/s and having operating conditions close to the typical ones suggested for recompression cycles. The novelty of the study, and the added value for the field of SCO_2 radial turbine research, is to investigate how well the loss predictions of different loss correlations, originally developed based on operation and designs of air/exhaust gas-driven turbines, and CFD results are in line with turbine designs having varied specific speeds. The specific speed range of 0.35 to 0.65 was selected as this range is typically considered for high-efficiency radial inflow turbine designs. Based on the results of the study, recommendations especially on using different correlations for predicting the rotor passage loss with different radial turbine design specific speeds are provided and discussed and the effect of turbine design rotational speed on the turbine loss distribution and flow field is highlighted. The main findings of the study can be exploited by researchers and engineers to select suitable loss correlations and to evaluate the accuracy of the different correlations for predicting losses of SCO_2 radial turbines. In addition, the results of this study can be utilized in the development of further improved loss models for SCO_2 turbomachines and in providing insights on the effect of the turbine design specific speed on the performance of SCO_2 cycles.

2. Materials and Methods

The turbine operating conditions for the study were selected based on previous studies for recompression SCO_2 cycles [23,24]. A turbine inlet temperature of 550 °C, inlet pressure of 200 bar, and outlet pressure of 75 bar were selected for the study as the turbine design

operating conditions. A design flow rate of 9 kg/s was used in defining the turbine geometries that correspond to about 1.05 to 1.1 MW turbine power depending on the turbine efficiency and design Ns. The methods for defining the turbine geometry and losses, the investigated turbine geometries as well as the methods used in the CFD analysis are described in this section. A radial-inflow turbine geometry, including the stator vanes and rotor, is presented in Figure 1a. An example of a typical velocity triangle shape at the rotor inlet is presented in Figure 1b.

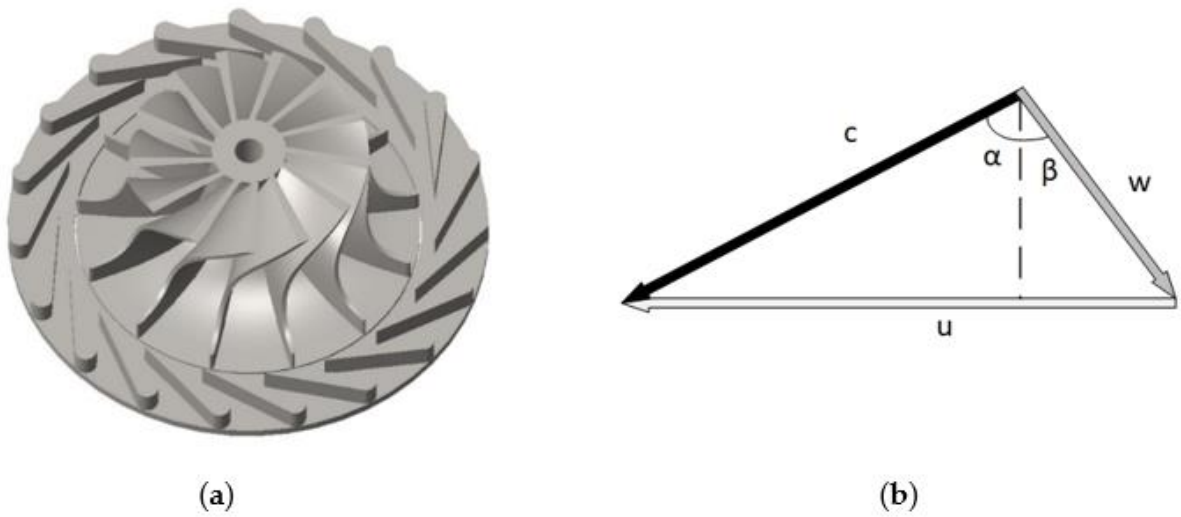

Figure 1. A radial-inflow turbine rotor geometry and stator vanes (**a**) and example of a typical rotor inlet velocity triangle (**b**).

2.1. Radial-Inflow Turbine Design

Radial inflow-turbines were designed by using the design approach and in-house code presented in the recent paper by Uusitalo et al., [16]. The mass flow rate, turbine inlet conditions, outlet static pressure and initial guess for the turbine efficiency were given as the inputs for the calculation. A commercial thermodynamic and transport property database Refprop [25] was used for defining the CO_2 thermodynamic properties in the turbine design. The stator dimensions and the rotor geometry were defined based on the given inputs. The geometry definition and loss calculations were based on solving the Euler turbomachinery equation, velocity triangles and the flow continuity equation at the stator outlet/rotor inlet and at the rotor outlet. The methods by Rohlik [26] and Balje [17] were followed in the turbine design, including the selection of the optimal flow angle at the stator outlet and the selection of the rotor diameter ratios for the design with different Ns. The diffuser or volute design were not taken into account in this analysis. Once the turbine geometry was defined, the losses were evaluated by using different enthalpy loss correlations. The new turbine efficiency obtained from the loss estimation was used to update the geometry definition. The calculation was iterated until no significant changes in the turbine geometry or in the predicted losses and isentropic efficiency between the iteration rounds were observed. The turbine isentropic efficiency is defined as

$$\eta_s = \frac{\Delta h}{\Delta h_s} = \frac{\Delta h_s - \Sigma \Delta h_{loss}}{\Delta h_s} \tag{1}$$

The specific speed can be expressed as

$$N_s = \frac{\omega \sqrt{q_v}}{\Delta h_s{}^{0.75}} \tag{2}$$

The losses that were considered in the turbine design were the stator loss, rotor passage loss, tip clearance loss, and incidence loss. In addition, the kinetic energy at

the rotor outlet was assumed as a loss since the use of the diffuser was not considered. The thermal losses or losses counted as parasitic losses, such as the disk friction loss, were not considered in this study as the analysis was concentrated on investigating the aerodynamic losses of the turbines. The used loss models represent the losses in a form of enthalpy loss. A summary of the used loss models and the corresponding literature references are summarized in Table 1. In the recent literature, different rotor passage loss models have been used for predicting losses in SCO_2 radial inflow turbines. In this study, three different loss models for the passage loss were included and compared. The model by Balje, referred to as PLM1 in this study, has been recently used for example in the studies by Lee et al. [27] and Uusitalo et al. [28]. The passage loss model by Wassenbauer and Glassman [29], referred to as PLM2 in this study, has been recently suggested by Lv et al. [6] for radial turbines using SCO_2 as the working fluid. The third loss model, referred to as PLM3, is the CETI model [30] that has been suggested to be used for SCO_2 radial turbines by Cho et al. [31] as this model takes into account the frictional effects in the rotor and the geometric information, including the angles of relative velocities as well as the magnitude of the relative velocities. The PLM3 was also recently used in the study by Uusitalo et al. [16] for predicting rotor losses in SCO_2 radial turbines with different design Ns. The other models that were selected for the study are the model of Whitfield and Baines [32] which is used for predicting the loss in the stator vanes, incidence loss model by Whitfield and Wallace [33], and tip clearance loss model by Jansen [34]. The exit kinetic loss was defined in the similar way as in [35].

Table 1. Summary of enthalpy loss correlations used in the radial turbine design.

Loss	Equation	Model/Source
Stator loss	$\Delta h_{stat} = 4 f_{nozzle} C_{avg}{}^2 \frac{L_{hyd,nozzle}}{D_{hyd,nozzle}}$	Whitfield and Baines [32]
Passage loss (PLM1)	$\Delta h_{pass} = \Phi^{1.75} \frac{(1+K_I)^2}{8} z_I U_2{}^2$ $z_I = 0.88 - 0.5\Phi$, $\Phi = C_{r1}/U_1$, $K_I = C_{r1}/C_{r2}$	Balje [27]
Passage loss (PLM2)	$\Delta h_{pass} = K(W_1{}^2 COS\beta_1{}^2 + W_2{}^2)/2$ $K = 0.3$	Wasserbauer and Glassman [29]
Passage loss (PLM3)	$\Delta h_{pass} = K_p \left(\frac{L_h}{D_h} + 0.68 \left[1 - \frac{R_{2m}}{R_1} \right] \frac{COS\beta_{2m}}{\frac{b_2}{c}} \right) 0.5 \left(W_1{}^2 + W_2{}^2 \right)$ $K_p = 0.11$, $c = Z/\cos\beta_{avg}$	Moustapha et al. [30]
Tip clearance loss	$\Delta h_{tc} = 0.6 \frac{t_c}{b_1} \sqrt{\frac{4\pi}{b_1 Z} C_{u1}{}^3 C_{r2} \frac{R_{2,tip}{}^2 - R_{2,hub}{}^2}{\left(R_1 - R_{2,tip}\right)\left(1 + \frac{\rho_1}{\rho_2}\right)}}$	Jansen [34]
Incidence loss	$\Delta h_{incidence} = 0.5 W_{u1}{}^2$	Whitfield and Wallace [33]
Exit kinetic loss	$\Delta h_{exit} = 0.5 C_2{}^2$	Rahbar et al. [35]

The complete description of the 1D design method, as well as the validation of the method, is presented in detail in [16]. The turbine design code was validated against the data available in the literature for supercritical CO_2-driven radial inflow turbines in [16] The PLM3 was used in this validation study. The design code was validated against the turbine designs presented by Qi et al. [8], Lv et al. [6] and Zhou et al. [7]. The comparison showed that there were only small deviations in the turbine geometries and efficiencies between the design code and the turbine designs presented in the literature. Deviations in the turbine radius from 0.3% to 6.8% and in blade heights of a maximum of below 10% was observed in the comparison. Deviations in the predicted turbine efficiencies from 0.3% to 4.9% were observed. The complete description of the code 1D validation is given in [16].

2.2. Investigated Turbine Geometries

The main geometric and operational parameters of the investigated turbines are presented in Table 2 and the turbine dimensions are obtained from the previous study by the authors [16]. The indicative stator and rotor geometries are shown in Figure 2a–d for the turbine designs with Ns = 0.35, 0.45, 0.55 and 0.65 to visualize how the different

design specific speeds affect the geometry and 3D profiles of the blades. With the designs with low Ns, the turbine wheel has a larger diameter, and the inlet blade height is lower when compared to the designs with high Ns. On the other hand, with high Ns designs the required rotational speed is significantly higher when compared to the low Ns designs. It should be noted that as the turbine geometrical design is connected to the turbine losses, the use of different loss correlations leads to minor differences also in the radial turbine geometry. The geometries presented in Table 2 are results of the turbine designs, where the blade passage loss was defined by using PLM3. The geometries presented in Table 2. were also used for generating the 3D geometries used in the CFD analysis.

Table 2. Main geometrical parameters of the investigated radial turbine designs.

Ns	0.35	0.4	0.45	0.5	0.55	0.6	0.65
n [krpm]	60.6	69.4	78.2	86.9	95.7	104.4	112.7
D_1 [mm]	110.4	97.3	86.9	78.5	71.5	65.2	59.5
b_1 [mm]	4.8	4.9	5.0	5.1	5.2	5.3	5.4
b_2 [mm]	16.7	16.8	16.8	16.9	16.9	16.0	14.6
D_2, tip [mm]	47.7	48.0	48.1	48.2	48.3	45.6	41.7
D_2, hub [mm]	14.3	14.4	14.4	14.5	14.5	13.7	12.5
α_1	78.8	77.7	76.7	75.6	74.5	73.5	72.4
Z [–]	16	15	14	14	13	12	12

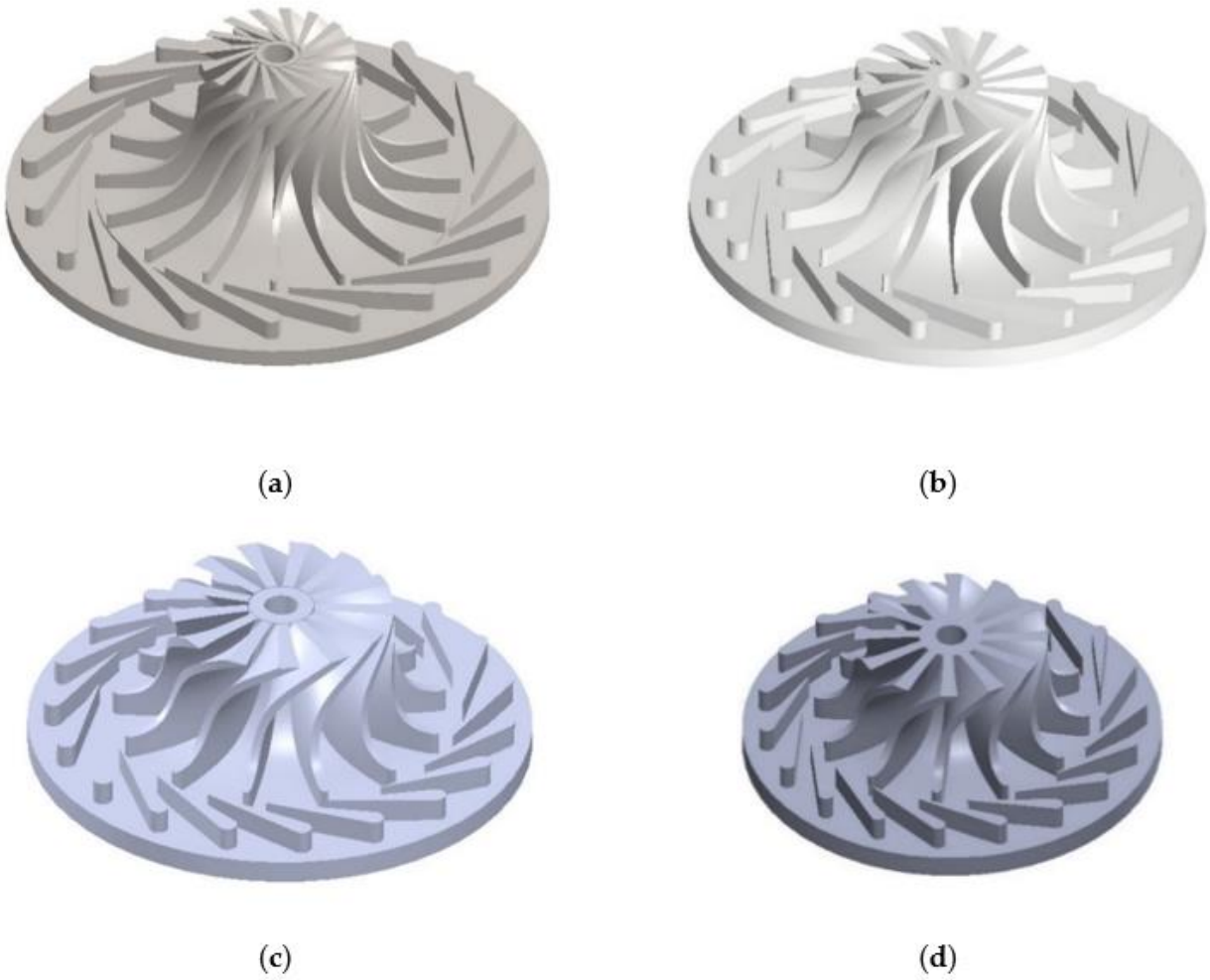

Figure 2. Turbine geometries with different specific speeds, (**a**) Ns = 0.35, (**b**) Ns = 0.45, (**c**) Ns = 0.55 and (**d**) Ns = 0.65.

2.3. CFD Analysis

A commercial software, Ansys CFX, was used as the flow solver in the CFD analysis. The turbine stator and rotor 3D geometries were generated based on the turbine 1D designs presented in [16] by using software, Ansys BladeGen and Solidworks. The computational grids of structured type were generated by using the Pointwise software. The CFD analysis was carried out for similar geometries with similar dimensions and blade angle distributions, as shown in Figure 2a–d, with the exception that slightly lower blade thicknesses were adopted in the CFD analysis, especially at the rotor outlet, when compared to the geometries presented in Figure 2a–d. This deviation can be explained by the fact that in the grid generation the inlet and outlet blade thickness was defined as a fraction of the rotor inlet and outlet diameter for each design case, whereas in the 3D geometries generated with Ansys BladeGen and presented in Figure 2a–d, a constant blade thickness of 2 mm was used for all the designs. In addition to the geometries presented in Figure 2a–d, the CFD simulations were done also for turbines with Ns = 0.4, 0.5, 0.6 as well as for a design with Ns = 0.57 that has been observed to reach the peak efficiency in the previous design study [16]. Thus, a total of 8 turbine geometries were investigated with the CFD analysis. The radial tip clearance height of 0.3 mm was used for all the grids and the axial clearance was in the same order of magnitude. The turbine stator and rotor losses were defined by comparing the enthalpy change in the CFD results to the isentropic ones, defined from the inlet conditions and outlet pressure.

The Reynolds averaged Navier-stokes (RANS) method was used and a two-equation shear stress transport turbulence model by Menter (k-ω SST) [36] was used in the CFD simulations. The total energy model including the viscous work was used. A frozen rotor interface approach to connect the stationary and rotational domains was used. The mass flow averaged flow quantities were monitored at the stator inlet section, between the rotor and stator, as well as at the rotor outlet. The simulation was kept running until there were no significant changes in the convergence residuals or in the inlet-outlet mass flows. The grid was refined near the walls, and a grid size near the walls of close to 1×10^{-6} m was used. The wall functions were enabled in the simulations in order to ensure the correct treatment method for the flow near the walls, depending on the local $y+$. An example of computational grid is presented in Figure 3a, and a more detailed example of the grid refinement near the stator nozzle walls and rotor blades is shown in Figure 3b. A single stator and rotor flow channel were modelled using the periodic boundary conditions for representing the periodicity of the geometry. The grid dependency study is presented and discussed in the next section.

The total temperature (550 °C) and total pressure (200 bar) were used as the inlet boundary conditions and the static pressure (75 bar) was used as the outlet boundary condition. The pressure boundary conditions were used in order to ensure equal pressure ratio and comparable isentropic enthalpy change for the different turbine designs. The thermodynamic properties of CO_2 were implemented to the flow solver by using a look-up table approach. The look-up table was generated by using the code by Ameli [37]. The thermodynamic properties in the look-up table were calculated by using the commercial thermodynamic database Refprop. More details on the method of using the look-up table and the effect of look-up table refinement on the CFD results with supercritical CO_2 radial turbines are given and discussed in [37,38]. The method for generating the look-up table by using the properties of Refprop is described in detail in [37]. The stator and rotor losses analyzed from the CFD results were gained by using the following procedure. First, the isentropic enthalpy at the turbine outlet was defined with Refprop by using the turbine inlet entropy and modelled turbine outlet pressure. The stator loss was defined from the CFD results by comparing the modelled static enthalpy at the stator outlet to the corresponding isentropic stator outlet enthalpy that was defined by using Refprop and the modelled stator outlet pressure and inlet specific entropy. Once the stator loss was defined, the rotor loss was defined by using the modelled enthalpy at the rotor discharge and comparing the

modelled enthalpy change over the turbine with the corresponding isentropic enthalpy change. The rotor loss was solved as,

$$\Delta h_{\text{rotor loss}} = \Delta h_2 - \Delta h_{2s} - \Delta h_{\text{stator loss}} \quad (3)$$

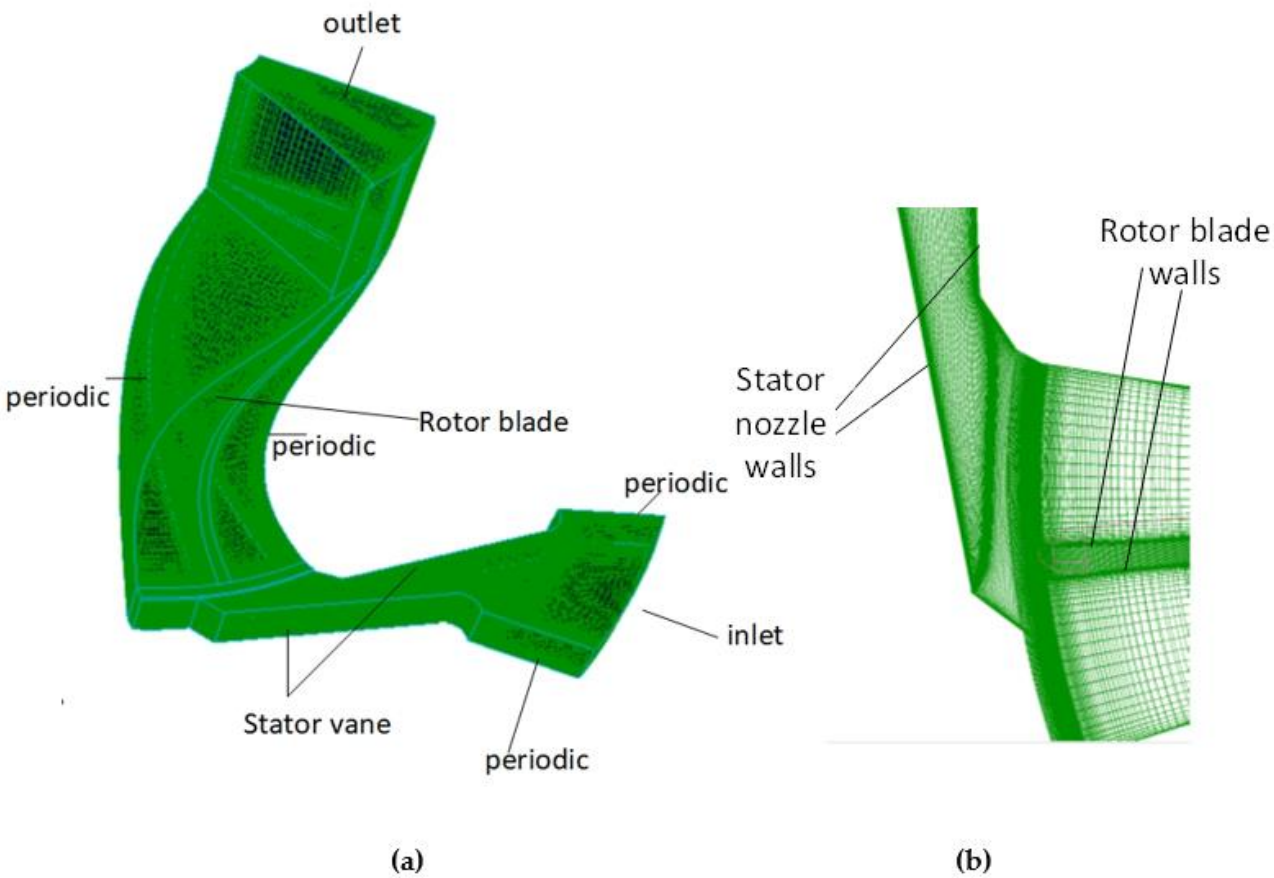

Figure 3. Example of (**a**) computational grid with one stator flow channel and one rotor flow channel modelled. (**b**) is showing an example of the grid refinement at the stator and rotor walls.

3. Results

In this section, the results and the main findings of the study are presented and analyzed. The results of the grid dependency study are presented first. Second, the CFD results and the results obtained with the loss correlations for the radial inflow-turbine designs with different design N_s are presented and compared.

3.1. Grid Dependency Study

The grid dependency study was carried out with three different grid sizes, to investigate the effect of the computational grid refinement on the CFD results. All the studied computational grids were of structured type. The turbine geometry with the specific speed of 0.55 was used in the grid dependency study. From the investigated grids, the coarse grid had total of about 0.4 million cells, medium grid had about 1.0 million cells and fine grid had about 2.4 million cells. The cell size at stator and rotor walls of 1×10^{-6} m were used with these grids. In addition, a fourth grid with the cell size at the walls of 1×10^{-7} m and having the number of cells comparable to the fine grid was investigated. This grid was included for having a comparison with a grid with lower $y+$ values and a higher number of cells within the boundary layer that reduces the need for using the wall functions near some location at the walls where the $y+$ was too high for modelling the flow without wall

functions. The results with the different grids on the flow quantities at the rotor outlet block were compared.

With the coarse grid, a deviation in outlet pressure of 0.0004% and a 0.26% deviation in temperature were detected when compared to the results obtained with the fine grid. With the medium grid, a 0.05% deviation in the pressure and a deviation of 0.1% in the temperature were detected when compared to the results obtained with the fine grid. A deviation of 1.6% was observed with the coarse grid and a deviation of 0.7% was observed with the medium grid in the turbine isentropic efficiency, excluding the exit kinetic loss, when compared to the results obtained with the fine grid. The deviations in the turbine outlet mass flow rate were below 1.5% between the different grids. The comparison of the results at the rotor discharge obtained with the different grids are shown in Table 3. Overall, there were rather small deviations in most of the main flow quantities between all the grids, and especially in the results between the medium and fine grids. In addition, the results between the two fine grids having different cell size near the walls had only minor differences in the results. The grid sizes comparable to the fine grid were used in the CFD analysis presented for the turbine designs with different Ns to avoid inaccuracies in the numerical results caused by the insufficient grid size, despite the fact that according to the grid dependency study, also the use of computational grids with a reduced number of nodes and with faster computational time would have led to acceptable accuracy in the CFD results.

Table 3. Grid dependency study. Results are shown for the properties at the rotor discharge. The relative differences presented in the table are compared to the results obtained with the fine grid.

Property	Coarse	Rel. Diff. %	Medium	Rel. Diff.%	Fine (Reduced y+)	Rel. Diff.%	Fine
s, [J/kgK]	2762.1	0.11	2760.4	0.05	2759.8	0.02	2759.1
h, [J/kg]	907,735	0.23	906,467	0.09	906,261	0.07	905,607
ρ [kg/m^3]	56.1	0.28	56.2	0.15	56.3	0.04	56.3
T [K]	707.23	0.26	706.14	0.1	705.98	0.08	705.4

3.2. Comparison of Loss Correlations and CFD Results

In this section, the results obtained with the loss correlations and CFD for the turbine losses with turbine designs with different N_s are compared and analyzed. Because it is difficult to distinguish the different individual loss mechanisms, especially in the complex 3D rotor flow in the CFD results, the comparison for the CFD and loss correlations is made for total stator losses, total rotor losses, and for exit kinetic losses, not otherwise considering the contribution of each individual loss mechanism in the CFD results.

The results of the CFD analysis and the 1D loss correlation for the stator loss are presented in Figure 4 with different design specific speeds. Both methods show that the stator loss is decreasing as the turbine design Ns is increased, even though all the stator designs are designed with similar mass flow, pressure ratio and outlet flow velocity of 370 m/s +/− 10 m/s. This can be explained by the fact that with high N_s designs, the stator frictional losses are decreased due to the reduced vane and stator hub and shroud surface areas caused by the smaller stator inlet and outlet diameters with high Ns designs. In general, the CFD analysis shows about 15% to 40% lower stator losses when compared to the results of the prediction of the 1D correlation. A constant stator vane solidity of 1.35 was used in the 1D correlation for each stator design, which can differ slightly from the final 3D geometries analyzed with the CFD. In addition, the 1D loss model does not take into account directly the effect of the vane trailing edge thickness. As the stator loss was observed to be sensitive on the trailing edge thickness, part of the scattering in the CFD results for the different stator designs might be also explained by the small differences in the vane trailing edge thicknesses and vane setting angles of the different geometries, that has an effect especially on the loss caused by the viscous wake leaving from the stator

vane trailing edge. The stator trailing edge thicknesses of about 0.3 mm to 0.4 mm were used in the investigated stator designs. If the trailing edge thickness was increased, the CFD results would become closer to the results of the 1D stator loss model. For example, by increasing the stator vane trailing edge thickness from 0.3 mm to 0.6 mm, the stator loss was increased from about 3.7 kJ/kg to over 5 kJ/kg in CFD analysis carried out for stator designs with N_s = 0.45. When decreasing the stator trailing edge thickness to below 0.1 mm the stator loss of about 3.3 kJ/kg was obtained. In addition, it should be noted that the 1D stator loss model considers the effect of surface roughness which has an effect on the predicted losses. The relative surface roughness of 0.0002 m was assumed in the 1D stator calculations. The effect of surface roughness was excluded in the CFD analysis since smooth walls were assumed in the CFD modelling. This fact can also at least partly explain why higher losses are predicted by the 1D correlation when compared to the CFD analysis, whereas the predicted trend for the stator losses with both methods is similar. When comparing the obtained stator loss results to the model by Benson [39], in where loss coefficients ranging from 0.05 to 0.15 are suggested for typical radial turbine stators [6], the obtained results for the stator loss are also well in line. The CFD results correspond to about 0.04 to 0.07 loss coefficients and the results of 1D correlation results correspond to about 0.05 to 0.12 loss coefficients, with an increasing loss coefficient value as the turbine design Ns is decreased.

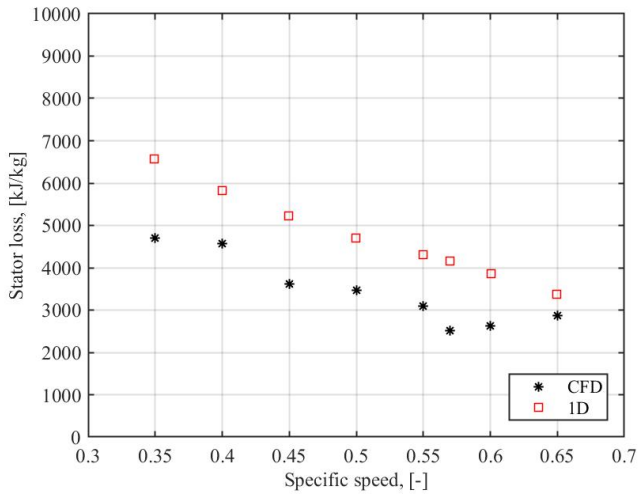

Figure 4. The comparison of CFD results and the results of 1D stator loss model.

The results on the passage loss obtained with CFD and with different passage loss models are shown in Figure 5. The passage loss presented includes the incidence loss, passage loss, and the tip clearance loss. Notable deviations in the predicted passage losses can be observed between the different passage loss models and the CFD. In general, when considering the investigated specific speed range, the best agreement between the CFD and 1D loss prediction was obtained when using the PLM3. The PLM1 and PLM2 both predict increasing losses as the turbine design specific speed is increased, whereas, with the PLM3, the lowest losses for the rotor are predicted for Ns values between 0.5 to 0.6. Of the studied passage loss models, with the investigated specific speeds, excluding the design with the lowest Ns of 0.35, the PLM3 have clearly the best agreement with the CFD results. For specific speeds of 0.45 and 0.5 both the PLM2, PLM3 and the CFD analysis results have only minor deviations observed between the results obtained with the different methods. With the low specific speed designs, the PLM3 shows also the best agreement in respect with the CFD results, but with the lowest Ns of 0.35 the deviation between the PLM3 model and CFD are notable as the rotor losses predicted in the CFD analysis were about 80 % of the losses predicted by the loss correlations. It is unclear what causes the notably lower losses in the CFD analysis with Ns = 0.35, when compared to the Ns = 0.4 and 0.45 designs,

as no significant differences in the flow fields and flow pattern between these different cases were observed when post-processing the results. One explanation could be that the Ns = 0.35 design has the highest number of blades, which can reduce the losses related to the flow separation in the rotor. In addition, the Ns = 0.35 has the lowest angle of relative velocity at the rotor outlet and it also has the highest relative clearances that influence the accuracy of the loss models. Based on the results, the PLM3 can be recommended to be used for predicting rotor losses in SCO_2 radial turbines, especially for the turbine designs having Ns ranging from 0.4 to 0.65. In addition, the PLM2 has good agreement between the model results and CFD especially at Ns 0.45 and 0.5. PLM1 has significant deviations when compared to the other models and CFD and based on the results, this model cannot be used for accurately estimating the passage losses with different specific speed designs, especially with low Ns turbine designs. However, with the highest investigated specific speeds from 0.55 to 0.65, the loss predictions of PLM1 and CFD are relatively close to each other.

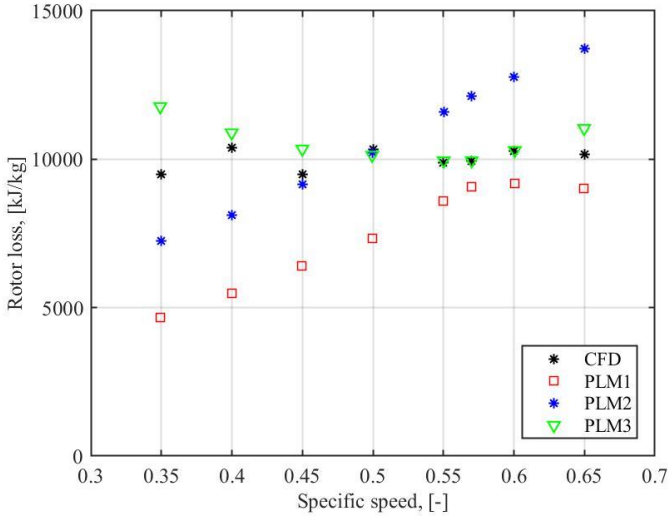

Figure 5. The comparison of CFD results and the results of different passage loss models of rotor losses including the passage loss, clearance loss and the incidence loss.

When considering the three different models, the PLM1 is based on only the velocities, whereas both the PLM2 and PLM3 take into account also the angle of the relative velocity (channel curvature). In addition, the PLM3 is the only one out of the three models that takes into account the actual dimension of the rotor, including the ratio of the outlet to inlet radius and blade height. In addition, the PLM3 takes into account the effect of the hydraulic length and hydraulic diameter in evaluating the losses. This could explain why the PLM3 resulted into best agreement with the CFD results for the different designs. The loss prediction of PLM2 could be improved by adjusting the coefficient K in the model as in this study the coefficient of 0.3 was used for all the investigated rotor geometries. This coefficient was defined based on the experiments with ideal gas-driven radial turbines [29], but it is unclear if this coefficient is valid for real gas turbines and especially for rotor designs with different specific speeds. Based on the obtained results, by using lower values for the coefficient for high Ns designs ($K \approx 0.2$) and higher values for low Ns designs ($K \approx 0.4$), the results of the PLM2 and CFD would be more in line. It should be also highlighted that the presented passage loss obtained with the CFD analysis includes the losses also caused by the tip clearance loss and incidence loss. Thus, the deviations in the predicted losses between the models and CFD are not only originating from the passage loss model but can be also caused by the inaccuracies in the tip clearance and incidence loss models for the different turbine design cases. It should be also emphasized that it is difficult to distinguish the contribution of different individual loss mechanisms from the CFD results due to the complex flow field of radial turbine rotors.

The results for the exit kinetic energy loss at the turbine rotor outlet, obtained with the 1D turbine design analysis and with the CFD are presented in Figure 6. In general, the exit kinetic loss is not significantly changing between the 0.35 to 0.57 specific speed designs as the rotor discharge flow area can remain comparable between these designs. This results to comparable rotor discharge velocities. With the turbine designs having the highest specific speeds, the maximum value of 0.7 for the inlet to outlet tip diameter ratio suggested by Rohlik [26] is reached, leading to increased exit kinetic loss as the specific speed is increased. There are also some deviations in the magnitude of exit kinetic loss calculated from the turbine 1D design and the CFD results, especially with the turbine design having the specific speed of 0.35 and 0.4. This can be partly explained by the small differences in the total blade blockage area used in the rotor outlet between the 1D calculation and CFD analysis. In addition, in the 1D turbine design the rotor discharge velocity was assumed to be completely axial, whereas in the CFD analysis results the rotor discharge flow is not completely axial in any of the designs but has a small swirl in the flow.

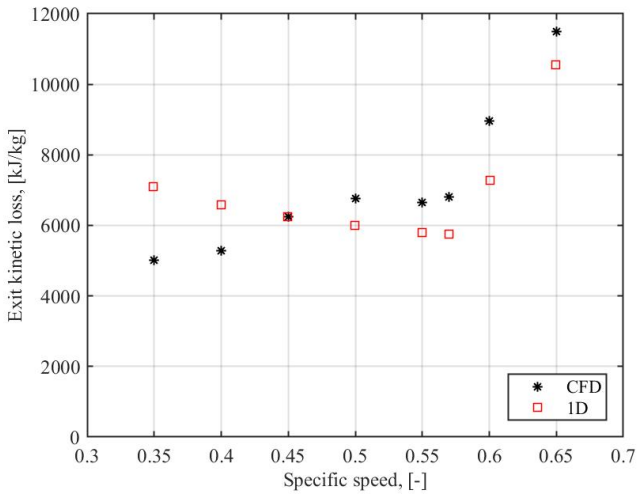

Figure 6. Turbine rotor exit kinetic loss predicted by using CFD and 1D design.

The turbine isentropic efficiency, excluding the exit kinetic loss, is presented in Figure 7a, and the efficiency, including the exit kinetic loss, predicted with the different loss correlations and CFD results, is presented in Figure 7b. In the CFD results, there are no significant changes in the CFD predicted efficiencies between the different designs having the specific speeds ranging from 0.35 to 0.6. Both the CFD method and the loss correlations predict that the efficiency is reducing quite notably when the turbine is designed for a specific speed greater than 0.6 if the exit kinetic energy is considered as a loss. This reduction is caused especially by the increasing rotor discharge velocity that results into high exit kinetic loss. In this study, the use of diffuser was not considered, and it is possible to increase the efficiency of especially the high Ns designs by recovering part of the kinetic energy at the rotor discharge with a diffuser. Even though the use of PLM3 resulted in the best agreement with the CFD results in predicting the rotor losses, the use of PLM3 results in notable deviation in the predicted turbine isentropic efficiency with low specific speed designs. This can be mainly explained by the fact that the stator losses predicted by the CFD are significantly lower than the ones predicted with the loss correlation, which increases the overall turbine efficiency significantly, especially with the low Ns designs in where the contribution of the stator loss is higher when compared to the designs with high Ns.

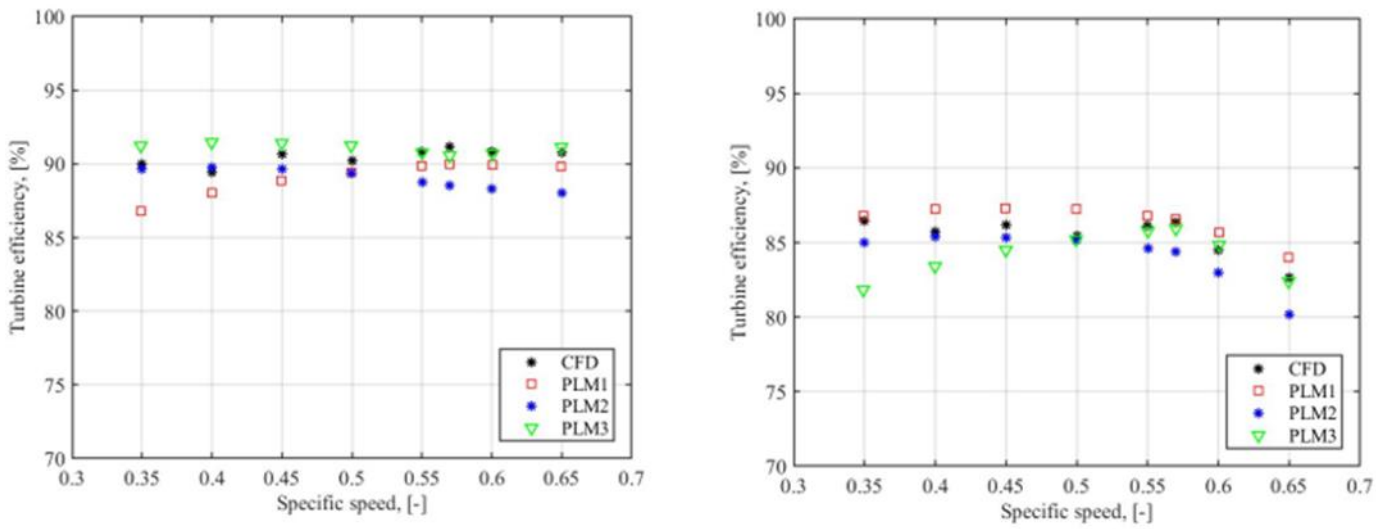

Figure 7. Turbine efficiency: (**a**) without the exit kinetic loss and (**b**) with exit kinetic loss.

The specific entropy contours for the turbine design with Ns = 0.45 is presented in Figure 8 to show the flow regions of the highest entropy generation and losses in the turbine. The main entropy generation regions are relatively similar for all the turbine designs and therefore the entropy contours are only shown for the Ns = 0.45 design. The velocity magnitude in the turbine stator and the rotor streamlines are presented in Figure 9a–d for Ns = 0.35, Ns = 0.45, Ns = 0.55 and Ns = 0.65 to visualize the flow acceleration in the stator and to present the streamlines in the rotor with designs having different specific speeds. In general, the flow has comparable flow structures with all the studied stator and rotor geometries. The viscous wake from the stator blade trailing edge causes some losses in the flow as can be observed as the increase in the specific entropy in Figure 8. In the streamlines presented in Figure 9a–d, the flow through the tip clearance gap can be clearly observed. In addition, there is a flow separation region starting near the rotor blade leading edge on the blade suction side that can be observed in the figures. This type of flow pattern can be considered as typical for radial inflow turbines and can be observed as a flow area with increasing specific entropy in Figure 8. This secondary flow structure in the blade suction side can also contain losses originating partly from the incidence loss, despite the fact that the contribution of the incidence loss can be considered to be rather low when running the turbine at design conditions. The main flow pattern is almost comparable in all the studied stator designs, except the small differences in the stator outlet flow angles and viscous wake thicknesses between the different cases. In general, the low Ns design leads to longer nozzles increasing the frictional losses, whereas in the high Ns turbine designs, the relative blockage of the stator vanes and the vane trailing edge becomes more significant, due to the smaller stator outlet diameter of high Ns design turbines. As the simulations were of steady type, the effects and losses related to the stator and rotor interaction were not considered.

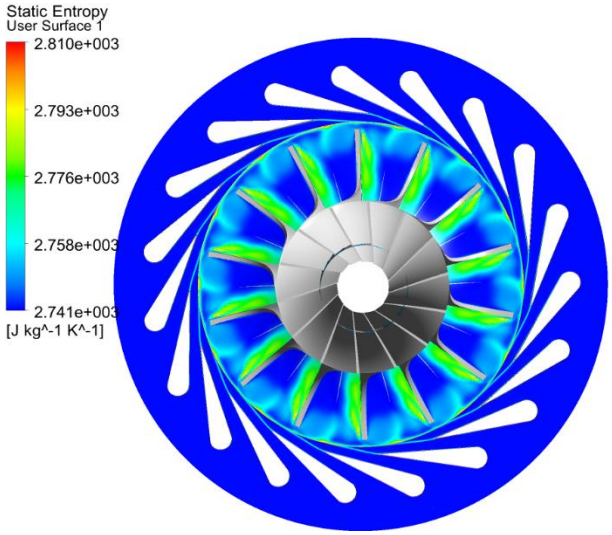

Figure 8. Example of specific entropy distribution in turbine stator and rotor. The contours are presented for design with specific speed of 0.45.

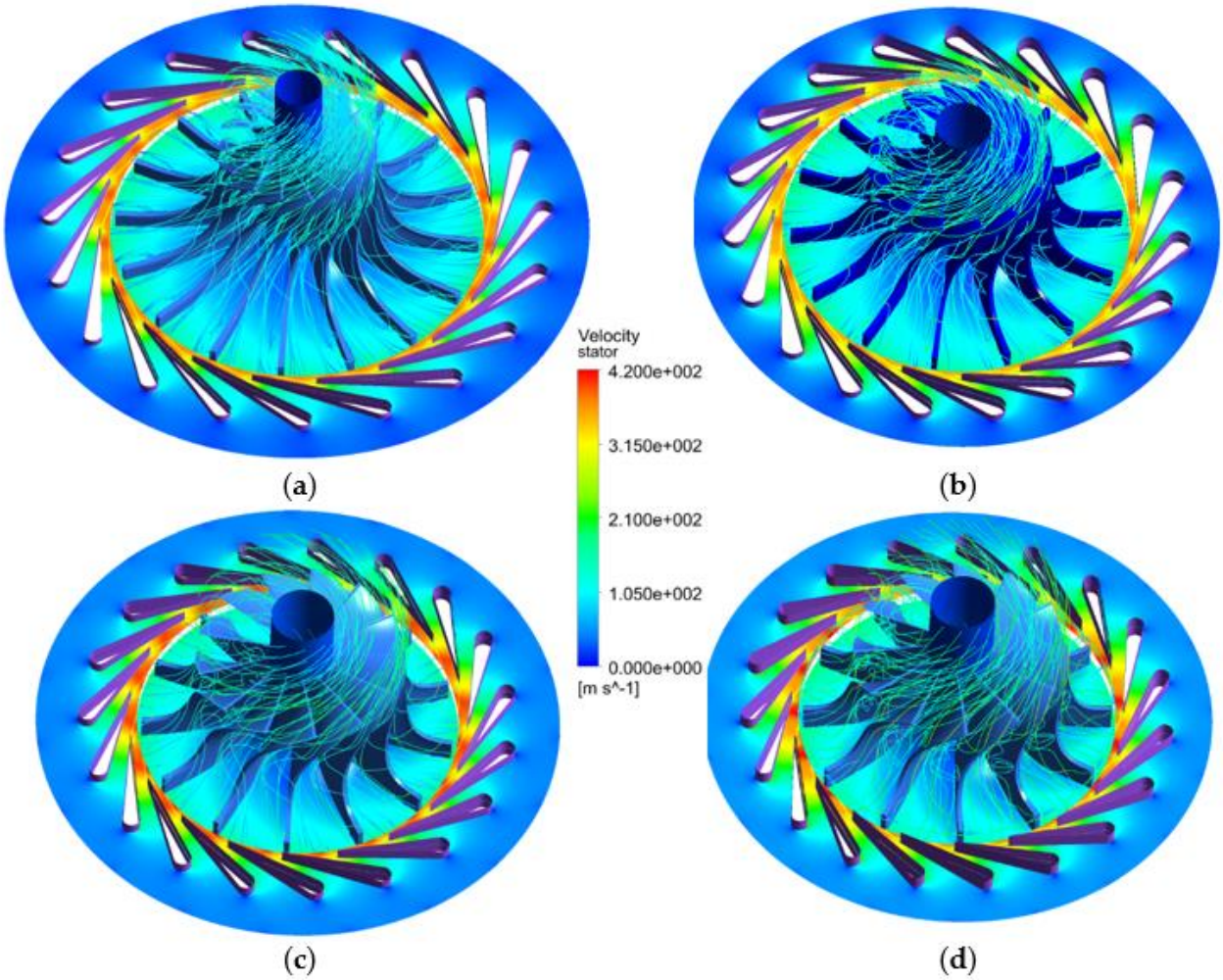

Figure 9. Effect of turbine design specific speed on turbine flow field, (**a**) Ns = 0.35, (**b**) Ns = 0.45, (**c**) Ns = 0.55 and (**d**) Ns = 0.65. In the stator the velocity magnitude is presented and the velocity scale in m/s is also given. In the rotor flow streamlines are shown in a rotating frame.

The different losses with the loss correlations using PLM3 passage loss model and the loss distribution obtained from the CFD analysis are presented in Figure 10a,b. The figures show that the total loss predictions between the two methods arein the same order of magnitude, especially with the specific speeds from 0.5 to 0.65. However, more notable differences between the methods are noticeable at lower specific speeds. It should be acknowledged, that the CFD rotor losses include also the incidence and the tip-clearance losses and their overall shares are comparable between the 1D and CFD approaches. The main reason for the observed discrepancies between the methods are especially caused by the differences in the precited stator and exit losses.

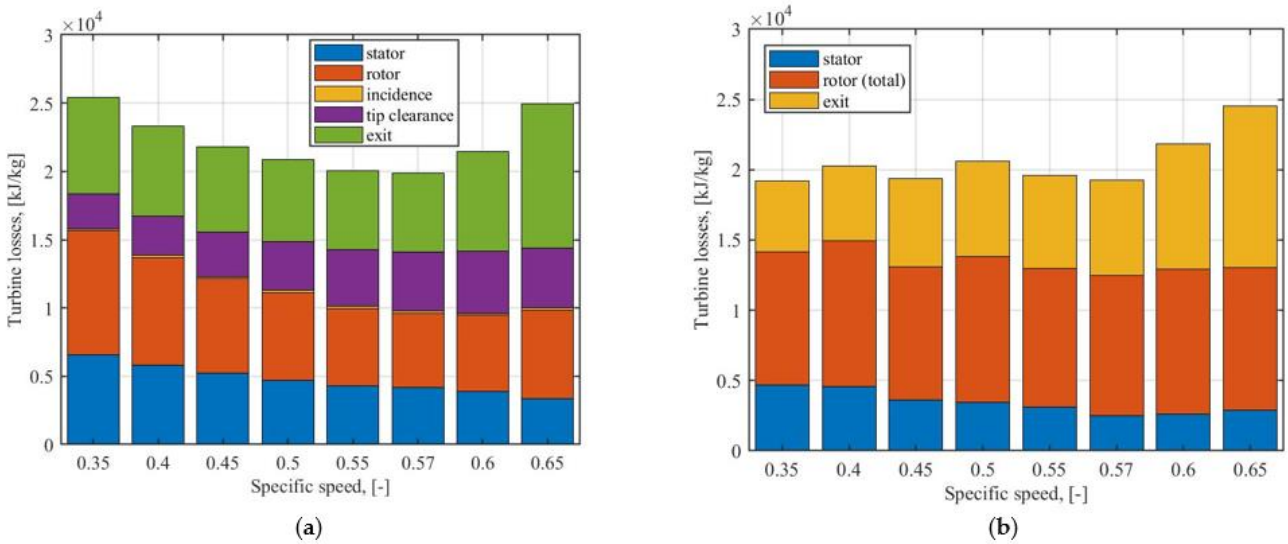

Figure 10. The turbine loss distributions (**a**) obtained with the loss models (PLM3) and (**b**) the CFD results for the losses.

4. Conclusions

A loss analysis for supercritical CO_2 radial inflow turbines with 9 kg/s design mass flow rate and having outputs close to 1 MW was carried out by using CFD and different loss correlations for predicting the turbine losses. The turbine designs having design Ns ranging from 0.35 to 0.65 were investigated. In general, both the use of loss correlations and the CFD analysis using 2-equation k-ω SST turbulence model had a relatively good agreement in the results. The stator loss model by Whitfield and Baines and the CFD results indicated similar trend for the decrease in the stator loss as the turbine design Ns was increased even though some differences in the predicted losses between the methods were observed. The effect of stator trailing edge thickness was observed to have significant effect on the stator loss and deviation between the CFD analysis and 1D model could be partly explained by the relatively sharp trailing edges used in the stator simulations. The use of three different rotor passage loss models were investigated and the results obtained by the correlations were compared to the results of the rotor losses of the CFD analysis. The CETI passage loss model, together with the incidence loss of Whitfield and Wallace and the tip clearance loss model by Jansen had the best agreement with the CFD results for predicting rotor losses, specifically with turbine designs having design Ns above 0.4. For the lowest investigated design specific speed of 0.35 a significant deviation in the losses estimated by CFD and the correlations were observed. Thus, the use of CETI loss correlation for the passage loss is recommended for SCO_2 radial turbine designs with a specific speed range of 0.4 to 0.65. In addition, the passage loss model by Wasserbauer and Glassman had a relatively good agreement with the CFD results, especially with specific speeds of 0.45 and 0.5. A better agreement with this model would have been reached by adjusting the coefficient K in the equation, especially for low and high specific speed designs. The results

obtained with the model by Balje and the CFD had significantly better agreement with the high specific speed designs when compared to the low specific speed turbine designs.

In future studies, the turbine losses are recommended to be studied with unsteady simulations, in order to include the effect of stator-rotor interaction on the expansion losses. It is also important to study and consider more in detail the manufacturability and strength limitations of the rotor blades and stator vanes, as the turbines have small dimensions and high rotational speeds. Thus, the effect of the stator vane trailing edge thickness and rotor blade thickness on the efficiency, mass flow and loss distribution is recommended to be included in future studies in more detail. Finally, it is worth highlighting that it is crucial to carry out more experimental studies on supercritical CO_2 radial turbines with different design specific speeds for validating and improving the accuracy of the numerical methods, as well as for developing further improved loss correlations for SCO_2 turbines for the improved prediction of the different losses.

Author Contributions: Conceptualization, A.U. and A.G.; Investigation, A.U. and A.G.; Methodology, A.U.; Project administration, A.U.; Writing—original draft, A.U. and A.G. All authors have read and agreed to the published version of the manuscript.

Funding: This study received funding from the Academy of Finland under project "Loss mechanisms in expanding supercritical fluids" (grant number 323248).

Data Availability Statement: The data presented in this study are available on request from the corresponding author. The data will be added on openly available repository later containing the research data of the project.

Conflicts of Interest: The authors declare no conflict of interest.

Nomenclature

U	peripheral velocity, m/s
C	absolute velocity, m/s
W	relative velocity, m/s
D	diameter, mm
b	blade height, mm
n	rotational speed, rpm
Z	number of blades, -
α	absolute flow angle
β	relative flow angle
t_c	tip clearance height, mm
η	efficiency, -
Ns	specific speed
h	enthalpy, kJ/kg
f	friction factor
L	length, mm
ω	angular speed, rad/s
q_v	volumetric flow rate, m^3/s
Subscripts	
0	stator inlet
1	stator outlet/rotor inlet
2	rotor outlet
h/hyd	hydraulic
m	meanline

References

1. Ahn, Y.; Bae, S.J.; Kim, M.; Cho, S.K.; Baik, S.; Lee, J.I.; Cha, J.E. Review of supercritical CO_2 power cycle technology and current status of research and development. *Nucl. Eng. Technol.* **2015**, *47*, 647–661. [CrossRef]
2. Allam, R.; Martin, S.; Forrest, B.; Fetvedt, J.; Lu, X.; Freed, D.; Brown, G.W.L.; Sasaki, T.; Itoh, M.; Manning, J. Demonstration of the Allam Cycle: An update on the development status of a high efficiency supercritical carbon dioxide power process employing full carbon capture. *Energy Procedia* **2017**, *114*, 5948–5966. [CrossRef]

3. Romei, A.; Gaetani, P.; Giostri, A.; Persico, G. The role of turbomachinery performance in the optimization of supercritical carbon dioxide power systems. *J. Turbomach.* **2020**, *142*, 071001. [CrossRef]
4. Saeed, M.; Alawadi, K.; Kim, S.C. Performance of Supercritical CO_2 Power Cycle and Its Turbomachinery with the Printed Circuit Heat Exchanger with Straight and Zigzag Channels. *Energies* **2021**, *14*, 62. [CrossRef]
5. Wang, Y.; Dostal, V.; Hejzlar, P. Turbine design for supercritical CO_2 brayton cycle. In *Global 2003*; American Nuclear Society: La Grange Park, IL, USA, 2003; pp. 1210–1220.
6. Lv, G.; Yang, J.; Shao, W.; Wang, X. Aerodynamic design optimization of radial-inflow turbine in supercritical CO_2 cycles using a one-dimensional model. *Energy Convers. Manag.* **2018**, *165*, 827–839. [CrossRef]
7. Zhou, K.; Wang, J.; Xia, J.; Guo, Y.; Zhao, P.; Dai, Y. Design and performance analysis of a supercritical CO_2 radial inflow turbine. *Appl. Therm. Eng.* **2020**, *167*, 114757. [CrossRef]
8. Qi, J.; Reddell, T.; Qin, K.; Hooman, K.; Jahn, I.H. Supercritical CO_2 radial turbine design performance as a function of turbine size parameters. *J. Turbomach.* **2017**, *139*, 081008. [CrossRef]
9. Fuller, R.; Preuss, J.; Noall, J. Turbomachinery for supercritical CO_2 power cycles. In Proceedings of the ASME Turbo Expo, Copenhagen, Denmark, 5–11 June 2012; Volume 44717, pp. 961–966.
10. Luo, D.; Liu, Y.; Sun, X.; Huang, D. The design and analysis of supercritical carbon dioxide centrifugal turbine. *Appl. Therm. Eng.* **2017**, *127*, 527–535. [CrossRef]
11. Lee, J.; Lee, J.I.; Ahn, Y.; Yoon, H. Design methodology of supercritical CO_2 brayton cycle turbomachineries. In Proceedings of the ASME Turbo Expo, Copenhagen, Denmark, 5–11 June 2012; pp. 975–983.
12. White, M.T.; Bianchi, G.; Chai, L.; Tassou, S.A.; Sayma, A.I. Review of supercritical CO_2 technologies and systems for power generation. *Appl. Therm. Eng.* **2021**, *185*, 116447. [CrossRef]
13. Pasch, J.; Conboy, T.; Fleming, D.; Rochau, G. *Supercritical CO_2 Recompression Brayton Cycle: Completed Assembly*; Sandia Report No. SAND2012-9546; Sandia National Laboratories (SNL): Albuquerque, NM, USA, 2012.
14. Holaind, N.; De Miol, M.; Saravi, S.S.; Tassou, S.A.; Leroux, A.; Jouhara, H. Design of radial turbomachinery for supercritical CO2 systems using theoretical and numerical CFD methodologies. *Energy Procedia* **2017**, *123*, 313–320. [CrossRef]
15. Son, S.; Jeong, Y.; Cho, S.K.; Lee, J.I. Development of supercritical CO_2 turbomachinery off-design model using 1D mean-line method and Deep Neural Network. *Appl. Energy* **2020**, *263*, 114645. [CrossRef]
16. Uusitalo, A.; Grönman, A.; Turunen-Saaresti, T. Design and loss analysis of radial turbines for supercritical CO_2 Brayton cycles. *Energy* **2021**, *230*, 120878. [CrossRef]
17. Balje, O.E. *Turbomachines—A Guide to Design Selection and Theory*; John Wiley: Hoboken, NJ, USA, 1981.
18. Rohlik, H.E. *Analytical Determination of Radial Inflow Turbine Design Geometry for Maximum Efficiency*; Nasa Technical Note; NTIS: Washington, DC, USA, 1968.
19. Unglaube, T.; Chiang, H.W.D. Preliminary Design of Small-Scale Supercritical CO2 Radial Inflow Turbines. *J. Eng. Gas Turbines Power* **2020**, *142*, 021011. [CrossRef]
20. Lee, S.; Gurgenci, H. A comparison of three methodological approaches for meanline design of supercritical CO2 radial inflow turbines. *Energy Convers. Manag.* **2020**, *206*, 112500. [CrossRef]
21. Persky, R.; Sauret, E.; Beath, A. Robust design and optimisation of a radial turbine within a supercritical co2 solar brayton cycle. In Proceedings of the 11th World Congress on Structural and Multidisciplinary Optimisation (WCSMO-11), Sydney, Australia, 7–12 June 2015; pp. 1–6.
22. Keep, J.A. On the Design of Small to Medium Scale Radial Inflow Turbines for Supercritical CO_2 Power Cycles. Ph.D. Thesis, The University of Queensland, Brisbane, Australia, 2019.
23. Sarkar, J. Second law analysis of supercritical CO2 recompression Brayton cycle. *Energy* **2009**, *34*, 1172–1178. [CrossRef]
24. Kulhanek, M.; Dostal, V. Supercritical carbon dioxide cycles thermodynamic analysis and comparison. In Proceedings of the International Symposium of Supercritical CO_2 Power Cycles, Pittsburgh, PA, USA, 27–29 March 2011; pp. 1–12.
25. Lemmon, E.W.; Huber, M.L.; McLinden, M.O. *NIST Standard Reference Database 23: Reference Fluid Thermodynamic and Transport Properties (REFPROP), Version 9.0*; National Institute of Standards and Technology: Gaithersburg, MD, USA, 2010.
26. Rohlik, H.E. Radial-Inflow Turbines. In *Turbine Design and Application*; Glassman, A.J., Ed.; NASA: Washington, DC, USA, 1972; Volume 290.
27. Lee, J.; Lee, J.I.; Yoon, H.J.; Cha, J.E. Supercritical carbon dioxide turbomachinery design for water-cooled small modular reactor application. *Nucl. Eng. Des.* **2014**, *270*, 76–89. [CrossRef]
28. Uusitalo, A.; Ameli, A.; Turunen-Saaresti, T. Thermodynamic and turbomachinery design analysis of supercritical Brayton cycles for exhaust gas heat recovery. *Energy* **2019**, *167*, 60–79. [CrossRef]
29. Wasserbauer, C.A.; Glassman, A.J. *FORTRAN Program for Predicting Off-Design Performance of Radial-Inflow Turbines*; NASA Technical Note Series; NASA: Washington, DC, USA, 1975.
30. Moustapha, H.; Zelesky, M.F.; Baines, N.C.; Japikse, D. *Axial and Radial Turbines*; Concepts ETI: White River Junction, VT, USA, 2003; Volume 2.
31. Cho, S.K.; Lee, J.; Lee, J.I. Comparison of Loss Models for Performance Prediction of Radial Inflow Turbine. *Int. J. Fluid Mach. Syst.* **2018**, *11*, 97–109. [CrossRef]
32. Whitfield, A.; Baines, N.C. *Design of Radial Turbomachines*; Longman Scientific and Technical: Essex, UK, 1990.

33. Whitfield, A.; Wallace, F.J. Study of Incidence Loss Models in Radial and Mixed-Flow Turbomachinery; Institution of Mechanical Engineers. In Proceedings of the Conference on Heat and Fluid Flow in Steam and Gas Turbine Plant, Coventry, UK, 3 April 1973.
34. Jansen, W. A Method for Calculating the Flow in a Centrifugal Impeller when Entropy Gradients are Present. In Proceedings of the Royal Society Conference on Internal Aerodynamics (Turbomachinery), Cambridge, UK, 19–21 July 1967.
35. Rahbar, K.; Mahmoud, S.; Al-Dadah, R.K.; Moazami, N. Modelling and optimization of organic Rankine cycle based on a small-scale radial inflow turbine. *Energy Convers. Manag.* **2015**, *91*, 186–198. [CrossRef]
36. Menter, F.R. Two-Equation Eddy-Viscosity Turbulence Model for Engineering Applications. *AIAA J.* **1994**, *32*, 1598–1605. [CrossRef]
37. Alireza, A. Supercritical CO_2 Numerical Modelling and Turbomachinery Design. Ph.D. Thesis, Lappeenranta University of Technology, Lappeenranta, Finland, 2019.
38. Ameli, A.; Uusitalo, A.; Turunen-Saaresti, T.; Backman, J. Numerical sensitivity analysis for supercritical CO2 radial turbine performance and flow field. *Energy Procedia* **2017**, *129*, 1117–1124. [CrossRef]
39. Benson, R.S. A review of methods for assessing loss coefficients in radial gas turbines. *Int. J. Mech. Sci.* **1970**, *12*, 905–932. [CrossRef]